ADVANCES IN APPLIED MATHEMATICS 5, 1–30 (1984)

A Generalized Riemann Problem for Quasi-One-Dimensional Gas Flows*,†

JAMES GLIMM,‡ GUILLERMO MARSHALL,‡ AND BRADLEY PLOHR

Department of Mathematics, The Rockefeller University, New York, New York, 10021

A generalization of the Riemann problem for gas dynamical flows influenced by curved geometry, such as flows in a variable-area duct, is solved. For this generalized Riemann problem the initial data consist of a pair of steady-state solutions separated by a jump discontinuity. The solution of the generalized Riemann problem is used as a basis for a random choice method in which steady-state solutions are used as an *Ansatz* to approximate the spatial variation of the solution between grid points. For nearly steady flow in a Laval nozzle, where this *Ansatz* is appropriate, this generalized random choice method gives greatly improved results.

1. INTRODUCTION

Many computational methods for solving gas flow problems are based on approximating the problem with a number of more elementary flow problems, called Riemann problems. The solutions of these Riemann problems are important because they provide an explicit and elementary class of solutions which contains extensive information about wave interaction. They are the basic constructive step in the random choice method, and they provide the key input into methods based on front tracking.

The solutions of Riemann problems for flows influenced by curved geometry exhibit, as characteristic phenomena, a bending and either strengthening or weakening of the waves. They may also contain waves

*A preliminary version of this paper was presented at the 1982 Army Numerical Analysis and Computers Conference, Vicksburg, Miss.

†This research was partially supported by the NSF, Grant PHY80-09179, by the ARO, Contract DAAG29-79-C-1079, and by the DOE, Contract DEA-Co2-76ER-03077.

‡Also at Courant Institute of Mathematical Sciences, New York University, New York, N.Y. 10012.

0196-8858/84 $7.50

completely missing when there is no curvature. Curvature effects arise, for instance, in one-dimensional flows in tubes with variable cross-sectional area and in flows with cylindrical and spherical symmetry. Such flows are called quasi-one-dimensional. Mathematically, the curved geometry introduces a source term in the conservation laws describing the flow, so that the conservation laws are inhomogeneous. This source term causes waves to change strength. Because the equations are quasi-linear, wave speeds depend on the wave strengths. Thus the trajectories of sound waves and shock waves are not straight lines when drawn in the space–time plane. For the conservation laws describing gas dynamics there is a nonlinear coupling of the modes of propagation, so that as a shock in a given mode changes strength, it emits signals which propagate in the other modes, leading to secondary waves [6, 7].

The initial data for the Riemann problem consist of a pair of constant states separated by a jump discontinuity. When there are no curvature effects (no source terms) the solution $\mathbf{w}$ of a Riemann problem depends only on $\xi = (x - x_{\text{jump}})/t$. In other words the solution $\mathbf{w}$ is scale, or similarity, invariant. The sound wave, shock wave, and particle trajectories are straight lines of the form $\xi = \text{const}$. Under the influence of curved geometry these trajectories bend as time progresses. The wave speeds and strengths, including those of secondary waves, depend on the source terms to first order in t, while the wave positions depend on the source terms only to second order in t.

To include second-order accuracy, the data for a Riemann problem are inadequate, however. The Riemann problem can be thought of as representing a localized portion of a complicated flow field. In order to obtain second-order accuracy of the Riemann problem solution it is necessary to give as data not only the values of the states on each side of the jump, but also their spatial derivatives. In other words, data which are accurate to first order are needed. For applications to two-dimensional front tracking, we imagine that a second-order finite difference method is used to obtain the solution on each side of the tracked front; we could thus obtain meaningful spatial derivatives for use in the Riemann problem data. In the context of the random choice method, however, this construction is not convenient. Instead we use a steady-state *Ansatz*; i.e., we suppose that over spatial mesh intervals the solution is a solution of the steady-state equations. This *Ansatz* allows us to extract first-order data from zeroth-order information, and to pose the problem of solving the Riemann problem to second order. This gives rise to what we call a generalized Riemann problem: an initial value problem with data consisting of two steady-state solutions separated by a jump discontinuity. Although it is possible to solve generalized Riemann problems to second order, we found it convenient to do somewhat less: curvature and strengthing of waves are included in our numerical solution,

but secondary waves are not included. Even this partial step is seen to give a remarkable improvement in the solution in cases where the steady-state *Ansatz* is appropriate. Our new method for solving inhomogeneous conservation laws incorporates this generalized Riemann problem into the framework of the random choice method; this constitutes what we call the generalized random choice method.

The purpose of this paper is to assess the benefits and difficulties of including second-order accuracy in the Riemann problem solution. For this purpose we studied gas flow in Laval nozzles using the generalized random choice method. We now describe the ordinary random choice method and its generalizations in more detail.

The random choice method is a technique for computing solutions of hyperbolic systems of conservation laws. It consists of approximating the solution at each time step by a piecewise constant state and advancing to the next time step by solving the local Riemann problems formed by the constant states on adjacent spatial mesh intervals. The value of the approximate solution over each mesh interval of the new time step is taken to be the exact solution evaluated at a randomly chosen point. The main advantages of the method lie in its power of resolution for the numerical treatment of discontinuities and sharp interfaces, and in its absence of over- and undershooting phenomena. The random choice method was introduced by Glimm [8] for homogeneous systems of conservation laws; it was developed into a numerical method by Chorin [2], who made extensive use of it for computations of combustion problems [3].

In its present form the random choice method cannot be applied to inhomogeneous hyperbolic systems of conservation laws, such as those describing quasi-one-dimensional gas flows. Several attempts have been made to extend the method to include these problems. Sod [17] developed a straightforward generalization using operator splitting. It consists of a two-step procedure. In the first step the inhomogeneous term is removed and the Riemann problem for the resulting homogeneous system is solved and sampled. In the second step the system of ordinary differential equations obtained by removing the convection terms is solved, using the solution from the first step as initial data. The advantages of this procedure are its simplicity and robustness. However, for certain applications, such as steady nozzle flows, this method requires that the mesh size be quite small to obtain reasonable accuracy.

Another generalization of the random choice method, which uses characteristic tracing, was developed by Marshall and Menendez [13]. This method, by contrast, is a one-step procedure. The Riemann problem for the associated homogeneous system is solved and the influence of the inhomogeneous term is introduced by integration along characteristic curves; only then is the solution sampled. The method of characteristic tracing is more

accurate than Sod's splitting method for equal mesh size, but the computational effort for obtaining the same degree of accuracy is greater for characteristic tracing.

Liu [11] has proved global existence for quasi-linear hyperbolic systems, including quasi-one-dimensional gas flow, using a method which generalizes that of Glimm. His results are limited, however, to gas flows which are nowhere sonic (but see Liu [12]). Fok [5] used this method as a basis for constructing a numerical scheme, which he called Liu's scheme. Here the solution at each time step is approximated by a piecewise steady flow. It is advanced to the next time step by solving the ordinary Riemann problems formed by the jumps between steady flow states on adjacent spatial mesh intervals (cf. the generalized random choice method described below). The approximating steady flow for each mesh interval at the new time step is obtained by sampling this solution at a randomly chosen point. Fok claims that this method offers only marginal improvement over Sod's method, and only at greater computational cost. In addition, it cannot handle transonic flows.

We now introduce the generalized random choice method. This method is also based on the work of Liu, but is an extension in two respects. Here again the solution at each time step is approximated by a piecewise steady flow. It is advanced to the next time step by solving, to second order in time, the generalized Riemann problems formed by the steady flows on adjacent spatial mesh intervals. (In practice, however, we did not include secondary waves.) The approximating steady flow for each mesh of the new time step is obtained by sampling this solution at a randomly chosen point. Thus we have extended Liu's methods to include the curving of shocks and rarefactions on the level of the local Riemann problem. We have also included a simple stabilizing mechanism in the numerical scheme which allows it to be applied to transonic flows.

The generalized random choice method was applied to transient gas flows, with and without shocks, in a Laval nozzle. We found significant improvement over finite difference methods as well as the above-mentioned generalizations of the random choice method. The major reason for this improvement seems to be that the random fluctuations caused by the sampling are greatly reduced: for nearly steady flows the solution is better approximated by piecewise steady flows than by piecewise constant flows.

The plan of the paper is as follows. In Section 2 we discuss the equations describing quasi-one-dimensional gas flows. In Section 3 we briefly review the random choice method. In Section 4 we introduce the generalized random choice method. In Section 5 we study the solutions of the steady-state equations in more detail. In Section 6 we present numerical results for gas flows in Laval nozzles. Finally, in Section 7 we draw some conclusions.

2. Quasi-One-Dimensional Gas Flow

We consider the one-dimensional flow of an inviscid, compressible, polytropic gas. The equations describing this flow may be written in the form

$$\mathbf{w}_t + \mathbf{f}(\mathbf{w})_x = \mathbf{g}(x, \mathbf{w}), \tag{2.1}$$

where

$$\mathbf{w} = \begin{pmatrix} \rho \\ m \\ e \end{pmatrix}, \qquad \mathbf{f}(\mathbf{w}) = \begin{pmatrix} m \\ m^2/\rho + p \\ (m/\rho)(e+p) \end{pmatrix},$$

$$\mathbf{g}(x, \mathbf{w}) = -\frac{\alpha'(x)}{\alpha(x)} \begin{pmatrix} m \\ m^2/\rho \\ (m/\rho)(e+p) \end{pmatrix},$$

and

$$\begin{aligned} \alpha(x) &= \textit{the cross-sectional area at } x && \text{for flow in a variable-area duct} \\ &= 2\pi x && \text{for cylindrically symmetric flow} \\ &= 4\pi x^2 && \text{for spherical symmetric flow.} \end{aligned}$$

Here ρ is the fluid's mass density, m is its momentum density ($m = \rho v$, where v is the fluid velocity), e is its (total) energy density, and p is the thermodynamic pressure, defined by the equation $e = m^2/2\rho + p/(\gamma - 1)$ for a polytropic gas with adiabatic constant γ. The three component equations of the system (2.1) express, respectively, the conservation of mass, Newton's law, and the conservation of energy.

We are interested in the general solution of the system (2.1) subject to initial conditions of the form

$$\mathbf{w}(x, t = t_0) = \mathbf{w}_0(x)$$

for all x, where the initial data $\mathbf{w}_0$ are prescribed. In our numerical method for obtaining general solutions certain special solutions, known as steady-state solutions, play a distinguished role. For a steady-state solution, $\mathbf{w}$ is independent of time, so that $\mathbf{w}_t = 0$ and $\mathbf{w}(x, t) = \mathbf{w}_0(x)$ for all x and t. Thus in order that $\mathbf{w}$ be a steady flow state it must satisfy the system of ordinary differential equations

$$\mathbf{f}(\mathbf{w})_x = \mathbf{g}(x, \mathbf{w}).$$

For example, in the case of flows in a duct with constant cross-sectional

area, where $\mathbf{g}(x, \mathbf{w}) = 0$, a steady flow must satisfy

$$\mathbf{f}(\mathbf{w})_x = 0,$$

so that

$$\mathbf{w}(x) = \mathbf{w}_{00}$$

for all x. In the general case the steady-state solutions may be obtained by solving the system of ordinary differential equations subject to a one-point initial condition

$$\mathbf{w}(x = x_0) = \mathbf{w}_{00}.$$

In this general case, however, steady-state solutions need not exist for arbitrary $\mathbf{w}_{00}$, and if they do exist they need not be unique. We shall discuss these features further in Section 5.

3. Review of the Random Choice Method

The random choice method is a numerical scheme for solving hyperbolic systems of conservation laws which is based on a constructive existence proof due to Glimm [8]. Consider the hyperbolic system

$$\mathbf{w}_t + \mathbf{f}(\mathbf{w})_x = 0 \tag{3.1}$$

subject to the initial conditions

$$\mathbf{w}(x, t = 0) = \mathbf{w}_0(x) \tag{3.2}$$

for all x. (Here $\mathbf{w}$ and $\mathbf{f}(\mathbf{w})$ are defined as in Section 2 if we are describing one-dimensional gas flow.) We introduce a space–time grid defined by mesh lengths Δx and Δt. The solution is to be calculated at points of the form $(x = i\,\Delta x, t = n\,\Delta t)$, where i and n are integers. Let us denote $\mathbf{w}(i\,\Delta x, n\,\Delta t)$ by $\mathbf{w}_i^n$. Because we impose the initial conditions (3.2) we know the values of $\mathbf{w}_i^0$ for all i; thus to specify the scheme it suffices to describe how $\mathbf{w}_i^{n+1}$ is calculated once $\mathbf{w}_{i-1}^n$, $\mathbf{w}_i^n$, and $\mathbf{w}_{i+1}^n$ are known. This is illustrated in Fig. 3.1 Consider the following initial-value problem, known as a Riemann problem,

$$\bar{\mathbf{w}}_t + \mathbf{f}(\bar{\mathbf{w}})_x = 0 \tag{3.3}$$

subject to the initial conditions

$$\begin{aligned} \bar{\mathbf{w}}(x, t = n\,\Delta t) &= \mathbf{w}_i^n \qquad \text{for } x < \left(i + \tfrac{1}{2}\right)\Delta x \\ &= \mathbf{w}_{i+1}^n \qquad \text{for } x \geqq \left(i + \tfrac{1}{2}\right)\Delta x. \end{aligned} \tag{3.4}$$

Assume that we can obtain the solution $\bar{\mathbf{w}}$ of this problem. Also assume that we have been given an equidistributed sequence ϑ_i of real numbers in the interval $[-\frac{1}{2}, \frac{1}{2}]$. Then if $\vartheta_i \geqq 0$ we define

$$\mathbf{w}_i^{n+1} = \bar{\mathbf{w}}\big((i + \vartheta_i)\,\Delta x, (n + 1)\,\Delta t\big),$$

while if $\vartheta_i < 0$ we define $\mathbf{w}_i^{n+1}$ in an analogous way in terms of the solution of the Riemann problem formed using $\mathbf{w}_{i-1}^n$ and $\mathbf{w}_i^n$ at $x = (i - \frac{1}{2})\,\Delta x$. By continuing this process the approximate solution is defined. Glimm proved that under certain assumptions the family of approximate solutions obtained by successively refining the grid will converge to a weak solution of Eq. (3.1). (The most important assumption, one that we will impose in our numerical implementation, is that the Courant–Friedrichs–Levy (CFL) condition be satisfied, viz., that $s_{\max}\,\Delta t \leqq \Delta x/2$, where $s_{\max}$ is the maximum wave speed of the solution.) This procedure may also be used to obtain numerical solutions of Eq. (3.1) if it is numerically feasible to solve the corresponding Riemann problems.

The solution of a Riemann problem is often much simpler to obtain than the solution of a general initial-value problem. This is essentially because both the equation (3.3) and the initial conditions (3.4) are invariant under the scaling transformation $(x, t) \to (x_{\text{jump}} + \alpha(x - x_{\text{jump}}), \alpha t)$; thus the solution depends only on the variable $\xi = (x - x_{\text{jump}})/t$, and the problem can be reduced to solving ordinary differential equations (for the smooth parts of the solution) and nonlinear equations (for the discontinuous parts of the solution). For gas dynamics the differential equations may be integrated, reducing the Riemann problem to a system of nonlinear equations. Here we briefly present the end result of this analysis so we may describe the general characteristics of the solutions of Riemann problems.

We will construct the solution of a Riemann problem by piecing together elementary waves. For gas dynamics there are three families of elementary waves:

1. *Rarefaction waves* are smooth solutions of the conservation laws. They are of two types, forward and backward (corresponding to the + and

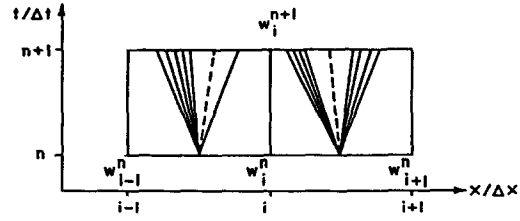

FIG. 3.1. The random choice mesh.

– cases below). In the space–time plane a rarefaction is a wedge separating two constant states, $\mathbf{w}_{\text{ahead}}$ and $\mathbf{w}_{\text{behind}}$. In the middle of the wedge the gas satisfies the following equations on the ray with slope

$$\xi = v \pm c,$$

where $c = (\gamma p/\rho)^{1/2}$ denotes the speed of sound:

$$v_{\text{ahead}} - v \pm \frac{1}{\gamma} c_{\text{ahead}} \cdot \frac{2\gamma}{\gamma - 1}\left[\left(\frac{p}{p_{\text{ahead}}}\right)^{(\gamma-1)/2\gamma} - 1\right] = 0 \qquad (3.5)$$

and

$$\frac{\rho}{\rho_{\text{ahead}}} = \left(\frac{p}{p_{\text{ahead}}}\right)^{1/\gamma}. \qquad (3.6)$$

The first equation states that the backward, respectively forward, Riemann invariants $r_{\mp} = \frac{1}{2}v \mp c/(\gamma - 1)$ are constant along the rays of forward, respectively backward, rarefactions. The second equation states that the thermodynamic entropy of the gas is constant throughout the rarefaction. Note that in order that the tail of the rarefaction not overtake the head it is necessary that $p_{\text{behind}} \leqq p_{\text{ahead}}$.

2. *Shock waves* are discontinuous (weak) solutions of the conservation laws. They are also of two types, forward and backward. In the space–time plane a shock is a discontinuity along the ray with slope

$$\xi = v_{\text{ahead}} \pm c_{\text{ahead}} \cdot \left[1 + \frac{\gamma + 1}{2\gamma}\left(\frac{p_{\text{behind}}}{p_{\text{ahead}}} - 1\right)\right]^{1/2}$$

that separates two constant states, $\mathbf{w}_{\text{ahead}}$ and $\mathbf{w}_{\text{behind}}$. These states are related by the equations

$$v_{\text{ahead}} - v_{\text{behind}} \pm \frac{1}{\gamma} c_{\text{ahead}} \cdot \frac{p_{\text{behind}}/p_{\text{ahead}} - 1}{\left[1 + \frac{\gamma + 1}{2\gamma}\left(\frac{p_{\text{behind}}}{p_{\text{ahead}}} - 1\right)\right]^{1/2}} = 0 \qquad (3.7)$$

and

$$\frac{\rho_{\text{behind}}}{\rho_{\text{ahead}}} = \frac{\frac{\gamma + 1}{\gamma - 1}\frac{p_{\text{behind}}}{p_{\text{ahead}}} + 1}{\frac{\gamma + 1}{\gamma - 1} + \frac{p_{\text{behind}}}{p_{\text{ahead}}}}. \qquad (3.8)$$

In order that the total entropy of the solution not decrease it is necessary that $p_{\text{behind}} \geqq p_{\text{ahead}}$.

3. *Contact discontinuities* are also discontinuous solutions of the conservation laws, but there is only one type. In the space-time plane a contact discontinuity is a discontinuity along the ray with slope $\xi = v_*$ separating two constant states which have the same fluid velocities v_* and the same pressure p_*, but different mass densities ρ_*^{left} and ρ_*^{right}.

The solution of the general Riemann problem consists of a backward rarefaction or shock on the left, a forward rarefaction or shock on the right, and a contact discontinuity in between. The particular case with a backward rarefaction and a forward shock is illustrated in Fig. 3.2. We call the states on the two sides of the initial jump discontinuity $\mathbf{w}_{\text{left}}$ and $\mathbf{w}_{\text{right}}$, and we denote by v_* and p_* the common values of velocity and pressure for the middle states on the two sides of the contact discontinuity. To write the equation which determines this solution it is convenient to introduce the function G defined by

$$G(\eta) = \frac{\eta - 1}{\left[1 + \frac{\gamma + 1}{2\gamma}(\eta - 1)\right]^{1/2}} \qquad \text{for } \eta \geqq 1$$

$$= \frac{2\gamma}{\gamma - 1}\left(\eta^{(\gamma-1)/2\gamma} - 1\right) \qquad \text{for } 0 \leqq \eta < 1.$$

Then from Eqs. (3.5) and (3.6) we see that the following two equations must hold:

$$v_{\text{left}} - v_* - \frac{1}{\gamma} c_{\text{left}} \cdot G\left(\frac{p_*}{p_{\text{left}}}\right) = 0 \tag{3.9}$$

and

$$v_{\text{right}} - v_* + \frac{1}{\gamma} c_{\text{right}} \cdot G\left(\frac{p_*}{p_{\text{right}}}\right) = 0. \tag{3.10}$$

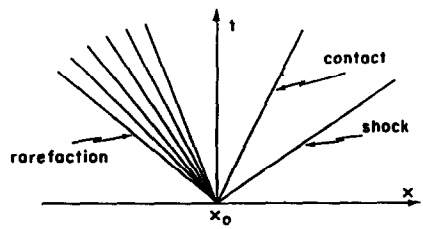

FIG. 3.2. The solution of an example of a Riemann problem with a backward rarefaction and a forward shock.

Eliminating v_* from these equations leaves us with a single nonlinear equation for p_*:

$$v_{\text{left}} - v_{\text{right}} = \frac{1}{\gamma} c_{\text{left}} \cdot G\left(\frac{p_*}{p_{\text{left}}}\right) + \frac{1}{\gamma} c_{\text{right}} \cdot G\left(\frac{p_*}{p_{\text{right}}}\right). \tag{3.11}$$

To solve the Riemann problem we thus use the following procedure: solve Eq. (3.11) for p_* and use Eq. (3.9) (or (3.10)) to obtain v_*; if $p_* \geq p_{\text{left}}$, so there is a backward shock, use Eq. (3.8) to determine ρ_*^{left}, while if $p_* < p_{\text{left}}$, so there is a backward rarefaction, use Eq. (3.6); similarly determine ρ_*^{right}; finally, in case there is a rarefaction wave in the solution, use Eqs. (3.5) and (3.6) to obtain the state of the gas in the middle of the rarefaction. (Of course some of these calculations may be omitted if the solution is to be determined at only one sample point.)

4. The Generalized Random Choice Method

We now describe a generalization of the random choice method which may be applied to inhomogeneous systems of conservation laws. Consider the inhomogeneous hyperbolic system

$$\mathbf{w}_t + \mathbf{f}(\mathbf{w})_x = \mathbf{g}(x, \mathbf{w}) \tag{4.1}$$

subject to the initial conditions

$$\mathbf{w}(x, t = 0) = \mathbf{w}_0(x)$$

for all x. We introduce a space–time grid, with mesh lengths Δx and Δt, in the same manner as in Section 3. Again let us denote $\mathbf{w}(i\,\Delta x, n\,\Delta t)$ by $\mathbf{w}_i^n$. As before it suffices to describe how $\mathbf{w}_i^{n+1}$ is calculated once $\mathbf{w}_{i-1}^n$, $\mathbf{w}_i^n$, and $\mathbf{w}_{i+1}^n$ are known. Consider the following initial-value problem, which we call a generalized Riemann problem,

$$\overline{\mathbf{w}}_t + \mathbf{f}(\overline{\mathbf{w}})_x = \mathbf{g}(x, \overline{\mathbf{w}})$$

subject to the initial conditions

$$\begin{aligned} \overline{\mathbf{w}}(x, t = n\,\Delta t) &= \mathbf{W}_{\text{left}}(x) \qquad \text{for } x < \left(i + \tfrac{1}{2}\right)\Delta x \\ &= \mathbf{W}_{\text{right}}(x) \qquad \text{for } x \geq \left(i + \tfrac{1}{2}\right)\Delta x \end{aligned}$$

where $\mathbf{W}_{\text{left}}$ and $\mathbf{W}_{\text{right}}$ are the solutions of the steady-state (ordinary differential) equations

$$\mathbf{f}(\mathbf{W})_x = \mathbf{g}(x, \mathbf{W}) \tag{4.2}$$

with initial conditions

$$\mathbf{W}_{\text{left}}(i\,\Delta x) = \mathbf{w}_i^n \qquad \text{and} \qquad \mathbf{W}_{\text{right}}((i+1)\,\Delta x) = \mathbf{w}_{i+1}^n.$$

Assume that we can obtain the solution $\bar{\mathbf{w}}$ of this problem. Also assume that we have been given an equidistributed sequence ϑ_i of real numbers in the interval $[-\frac{1}{2}, \frac{1}{2}]$. Then if $\vartheta_i \geqq 0$ we define

$$\mathbf{w}_i^{n+1} = \bar{\mathbf{w}}((i + \vartheta_i)\,\Delta x, (n + 1)\,\Delta t),$$

while if $\vartheta_i < 0$ we define $\mathbf{w}_i^{n+1}$ in an analogous way in terms of the solution of the generalized Riemann problem formed using $\mathbf{w}_{i-1}^n$ and $\mathbf{w}_i^n$ at $x = (i - \frac{1}{2})\,\Delta x$. By continuing this process the approximate solution is defined.

Liu [11] introduced a version of this scheme and used it to prove the existence of global weak solutions of Eq. (4.1). He showed that under certain assumptions the family of approximate solutions obtained by successively refining the grid will converge to a weak solution. To prove his result it sufficed to use an approximation to the solution $\bar{\mathbf{w}}$ of the generalized Riemann problem: an exact solution inside rarefaction waves is used, but neither the curvature of shock trajectories nor secondary waves were included. These existence theorems were limited, however, to flows which are nowhere sonic, because the differential equations (4.2) are singular when the gas approaches sonic conditions.

We have used another version of this scheme to obtain numerical solutions for certain gas flows. We have approximated the solution $\bar{\mathbf{w}}$ of the generalized Riemann problem in the following way: the solution inside a rarefaction wave is obtained to second order in Δt, and the second-order curving of the shock trajectories is included.

Let us describe the basic features of solutions to generalized Riemann problems. A particular example is shown in Fig. 4.1, where the area variation $\alpha'(x_0)$ is taken to be positive. A pressure–space–time diagram for a shock moving into a steady-state region is shown in Fig. 4.2. In contrast to the case of the ordinary Riemann problem, the states $\mathbf{W}_{\text{left}}$ and $\mathbf{W}_{\text{right}}$ now vary in space, being solutions of Eq. (4.2). Similarly, the states immediately to the left and right of the contact discontinuity will vary in space. To first order they may be approximated by steady-state solutions that attain, at

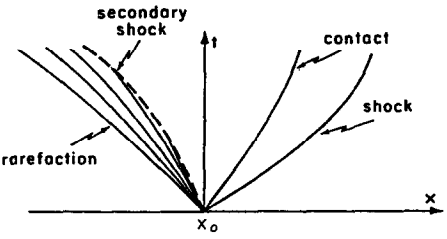

FIG. 4.1. The solution of an example of a generalized Riemann problem. Here $a'(x_0) > 0$.

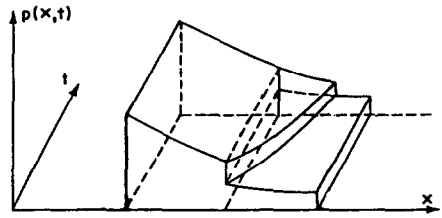

FIG. 4.2. p-x-t diagram of a single jump separating two steady-state regions and entering into a diverging cross-sectional area.

$x = x_0$, the states given by the solution of the ordinary Riemann problem. The initial slopes of the shock and contact discontinuities, as well as the head and tail of the rarefaction waves, are the same as those obtained by solving the ordinary Riemann problem for system (3.1) without source terms, where the constant-state initial conditions are given by $\mathbf{w}_{\text{left}} = \mathbf{W}_{\text{left}}(x_0)$ and $\mathbf{w}_{\text{right}} = \mathbf{W}_{\text{right}}(x_0)$. To curve the shock we solve the ordinary differential equation $dx/dt = \xi(x)$ for the shock position, where $\xi(x)$ is the shock velocity. For the example shown in Fig. 4.2 this equation reads

$$\frac{dx}{dt} = v_{\text{right}}(x) + c_{\text{right}}(x) \cdot \left[1 + \frac{\gamma + 1}{2\gamma}\left(\frac{p_*(x)}{p_{\text{right}}(x)} - 1\right)\right]^{1/2}$$

with the initial conditions $x(t = 0) = x_0$. In the same way the backward characteristics in the backward rarefaction may be curved by solving the ordinary differential equations

$$\frac{dx}{dt} = v(x) - c(x)$$

with the initial conditions $x(t = 0) = x_0$, where the variation of v and c in x is determined by solving the steady-state equations with initial conditions determined from the solution of the ordinary Riemann problem. In general there are also secondary waves, with strengths which are first order in Δt, that arise from the curvature [6, 7]. In Fig. 4.1, for instance, the slowing of the expanding shock results in backward compression waves which form a backward shock when they collide with the backward rarefaction. In our numerical scheme we have not included these effects, however.

5. STEADY-STATE SOLUTIONS IN GAS DYNAMICS

In this section we describe the properties of the steady-state solutions of the system (4.1) in more detail. We first consider smooth steady-state

solutions, i.e., solutions of the system of ordinary differential equations,

$$\begin{aligned} m_x &= -\frac{\alpha'(x)}{\alpha(x)} m, \\ \left[\frac{m^2}{\rho} + p\right]_x &= -\frac{\alpha'(x)}{\alpha(x)} \frac{m^2}{\rho}, \\ \left[\frac{m}{\rho}(e+p)\right]_x &= -\frac{\alpha'(x)}{\alpha(x)} \left[\frac{m}{\rho}(e+p)\right], \end{aligned} \tag{5.1}$$

subject to the initial conditions that $(\rho, m, e) = (\rho_0, m_0, e_0)$ at $x = x_0$. The first and the last equations may be integrated immediately to obtain

$$m\alpha(x) = m_0\alpha(x_0)$$

and

$$m\alpha(x)\frac{e+p}{\rho} = m_0\alpha(x_0)\frac{e_0+p_0}{\rho_0}.$$

Using the relations $m = \rho v$ and $e = m^2/2\rho + p/(\gamma - 1)$, these two equations may be rewritten

$$\rho v\alpha(x) = \rho_0 v_0 \alpha(x_0)$$

and

$$\frac{1}{2}v^2 + \frac{\gamma}{\gamma - 1}\frac{p}{\rho} = \frac{1}{2}v_0^2 + \frac{\gamma}{\gamma - 1}\frac{p_0}{\rho_0}.$$

These equations state that the mass flux and the total energy are constant throughout a steady flow. The second equation in the system (5.1) may be integrated after some manipulations, but it is simplest to note that the flow must be isentropic since there are no shocks. Thus the equation must state that the entropy is constant throughout a steady flow. Using the relation $p = A(S)\rho^\gamma$, where S is the entropy, we find the solution of system (5.1) to be equivalent to solving the following system of nonlinear equations,

$$\begin{aligned} \rho v\alpha &= \rho_0 v_0 \alpha_0, \\ \frac{p}{\rho^\gamma} &= \frac{p_0}{\rho_0^\gamma}, \end{aligned} \tag{5.2}$$

and

$$\frac{1}{2}v^2 + \frac{\gamma}{\gamma - 1}\frac{p}{\rho} = \frac{1}{2}v_0^2 + \frac{\gamma}{\gamma - 1}\frac{p_0}{\rho_0},$$

where $\alpha = \alpha(x)$ and $\alpha_0 = \alpha(x_0)$.

It is now convenient to introduce the speed of sound $c = (\gamma p/\rho)^{1/2}$ and the Mach number $M = v/c$. In terms of M, p, and c, the system (5.2) reads

$$\begin{aligned} Mpc^{-1}\alpha &= M_0 p_0 c_0^{-1}\alpha_0, \\ p^{\gamma-1}c^{-2\gamma} &= p_0^{\gamma-1}c_0^{-2\gamma}, \end{aligned} \tag{5.3}$$

and

$$\left(1 + \frac{\gamma - 1}{2}M^2\right)c^2 = \left(1 + \frac{\gamma - 1}{2}M_0^2\right)c_0^2.$$

The variables p and c may now be easily eliminated from system (5.3), leaving a single equation for M:

$$\frac{M}{\left(1 + \frac{\gamma - 1}{2}M^2\right)^{(\gamma+1)/2(\gamma-1)}}\alpha = \frac{M_0}{\left(1 + \frac{\gamma - 1}{2}M_0^2\right)^{(\gamma+1)/2(\gamma-1)}}\alpha_0. \tag{5.4}$$

The solution of the steady-state equations is thus reduced to the following procedure: solve Eq. (5.4) for M, use the last equation of system (5.3) to obtain c, use the second equation in system (5.3) to obtain p, and finally use the relation $c^2 = \gamma p/\rho$ to obtain ρ.

Let us now examine Eq. (5.4), which we rewrite as

$$F(M) = \frac{\alpha_0}{\alpha}F(M_0), \tag{5.5}$$

where the function F is defined by

$$F(M) = M\left(\frac{(\gamma + 1)/2}{1 + ((\gamma - 1)/2)M^2}\right)^{(\gamma+1)/2(\gamma-1)}$$

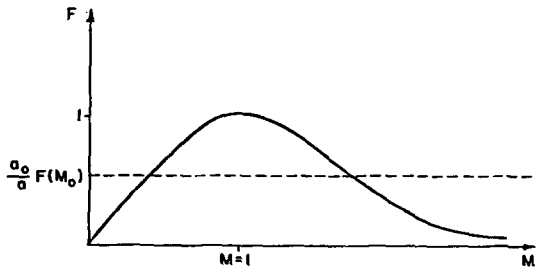

FIG. 5.1. Graph of the function defined in Eq. (5.5).

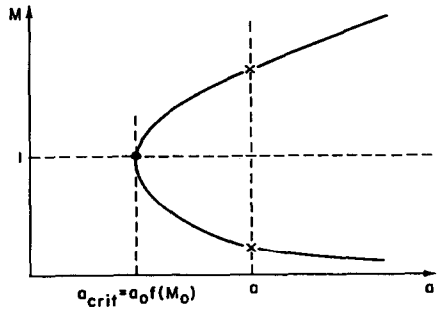

FIG. 5.2. Graph of the Mach number M versus area a for the solution of the equation $f(M) = a_{crit}/a$.

It is elementary to verify that F has the following properties:

$$F(0) = 0; \qquad F(M) \to 0 \quad \text{as} \quad M \to \infty;$$

$$F \text{ attains its unique maximum at } M = 1; \qquad F(M = 1) = 1.$$

The graph of F is shown in Fig. 5.1. Thus we see that there are two difficulties in solving Eq. (5.5): (1) if $\alpha < \alpha_0 F(M_0)$, no solution exists, since the right side of Eq. (5.5) exceeds the maximum value of F; and (2) if $\alpha > \alpha_0 F(M_0)$, there are two solutions of Eq. (5.5), one with $M > 1$ and one with $M < 1$, since a horizontal line drawn on the graph of F intersects F at two points. The graph of the Mach number versus area is shown in Fig. 5.2.

These results may be used to construct steady-state solutions for flow in a converging–diverging nozzle, such as that shown in Fig. 5.3. In order that a steady-state solution exists in the converging section of the nozzle we must have

$$\alpha_{\text{throat}} \geqq \alpha_{\text{inlet}} F(M_{\text{inlet}}).$$

In other words, we must have $M_{\text{inlet}} \geqq M_{\text{critical}}^{\text{supersonic}}$ or $M_{\text{inlet}} \leqq M_{\text{critical}}^{\text{subsonic}}$, where the supersonic and subsonic critical Mach numbers are the two solutions of the equation $F(M_{\text{critical}}) = \alpha_{\text{throat}}/\alpha_{\text{inlet}}$. The graph of Mach number versus distance along the nozzle for these allowed inlet Mach numbers is shown in Fig. 5.4. The lower family of curves corresponds to subsonic flow throughout the nozzle, with a rise in flow speed at the throat (this is Bernoulli's principle); the upper family of curves corresponds to supersonic flow throughout the nozzle. The critical curves corresponding to $M_{\text{inlet}} = M_{\text{critical}}^{\text{supersonic}}$ and to $M_{\text{inlet}} = M_{\text{critical}}^{\text{subsonic}}$ meet at the throat, where $M = 1$. Thus, for example, there are two solutions of the system of ordinary differential equations (5.1) such that $M_{\text{inlet}} = M_{\text{critical}}^{\text{subsonic}}$: one for which the

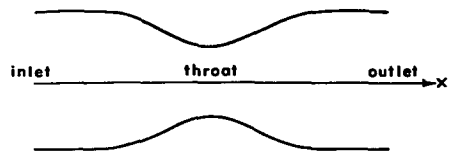

FIG. 5.3. A Laval nozzle.

flow is subsonic throughout, and another for which the flow is subsonic at the inlet but supersonic at the outlet. Thus there is a branching, or nonuniqueness, for steady flows which pass through the sonic point where the Mach number is unity.

We remark that the critical curves indeed have zero slope at the throat, despite what might be inferred from Fig. 5.2. In fact, the derivative of M with respect to α diverges only as $(\alpha - \alpha_{\text{crit}})^{-1/2}$, while the derivative of α with respect to x vanishes as $x - x_{\text{throat}} \sim \alpha - \alpha_{\text{crit}}$ (assuming a smooth nozzle), so that the derivative of M with respect to x vanishes at the throat.

In order to obtain steady-state solutions which allow outlet Mach numbers other than those shown in Fig. 5.4 it is necessary to allow standing shocks to form in the outlet of the nozzle. Solutions of this form have three different regions: a subsonic region in the inlet, which follows the subsonic critical curve up to the throat; a supersonic region, following the supersonic critical curve of Fig. 5.4 from the throat to the shock position; and a subsonic region behind the shock, which follows a subsonic steady-state solution corresponding to an outlet Mach number exceeding the critical one. Examples of such solutions are depicted in Fig. 5.5. The various solutions are parametrized by the shock position, or equivalently the shock strength, outlet Mach number, or outlet pressure (back pressure).

These solutions are obtained theoretically as follows. Given the position of the shock in the outlet, together with inlet conditions which are critical for the nozzle (so $M_{\text{inlet}} = M_{\text{critical}}^{\text{subsonic}}$), the flow in the region ahead of the

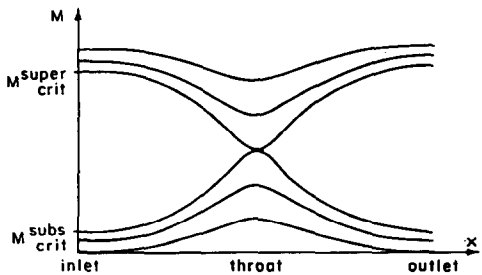

FIG. 5.4. Various graphs of the Mach number versus distance along the nozzle for shockless steady flows.

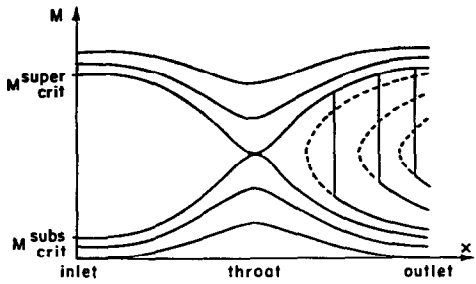

FIG. 5.5. Various graphs of Mach number versus distance along the nozzle for steady flows with a standing shock at the exit.

shock is determined by solving the steady-state equations; this flow corresponds to subsonic critical flow ahead of the throat and supersonic critical flow between the throat and the shock. To obtain the state behind the shock one imposes the Rankine–Hugoniot relations for a standing shock, namely, that the mass flux does not change across the shock, and that the momentum and energy fluxes change only according to the pressure drop across the shock, as determined by Newton's law. This gives three equations which determine the state just behind the shock, having given the state just ahead of it. Finally the flow downstream of the shock is determined by solving the steady-state equations for that steady flow which passes through the state behind the shock.

From Fig. 5.5 it would seem possible that there be a solution which is supersonic at the inlet, subsonic between the throat and the shock, and supersonic again behind the shock; but such a shock would violate the entropy condition. (The entropy condition is equivalent to the requirement that the flow ahead of the standing shock be supersonic.) There are, however, solutions with a shock at the inlet for which the flow is supersonic ahead, subsonic and critical between the shock and the throat, and supersonic and critical downstream of the throat. We do not consider these solutions further in this work.

Let us make some remarks about the boundary conditions that are appropriate for gas flows in a nozzle. At the inlet of the nozzle the fluid moves subsonically from left to right. Thus there are two families of characteristics, the forward sound waves and the particle paths, which leave the boundary and enter the region of computation; consequently two independent boundary equations must be imposed at the inlet. We have chosen to require that both the total temperature T, given by

$$kT = \frac{1}{2}v^2 + \frac{\gamma}{\gamma - 1}\frac{p}{\rho},$$

and the thermodynamic entropy S, or equivalently the function $A(S)$ given by $p = A(S)\rho^{\gamma}$, remain constant at the inlet throughout the time evolution. At the outlet, however, only the backward sound waves leave the boundary and enter the computational region, so only one boundary equation may be imposed. We have chosen to fix the outlet (or back) pressure of the nozzle.

6. Numerical Results

We present the results of numerical tests using the generalized random choice method applied to the problem of transient gas flows which possesses an asymptotic steady state whose solution is known. We compare these results with those obtained using Sod's splitting method and finite difference methods.

In the numerical tests we considered the flow of an inviscid, polytropic, compressible gas through a convergent–divergent (Laval) nozzle. The nozzle, taken from Moretti [14], was composed of four parts, each of length 5.0: an inlet section area 1.0, a sinusoidal expansion from the throat back to area 1.5, and an outlet section of constant area.

We present two series of numerical experiments. The first series involves a transient gas flow which approaches a completely subsonic steady-state flow

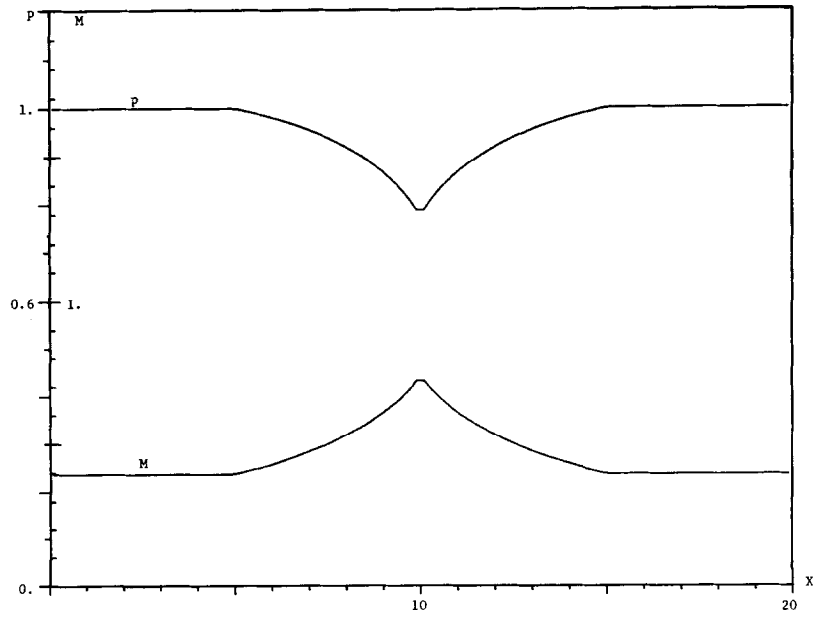

Fig. 6.1. Initial conditions for the first series of runs.

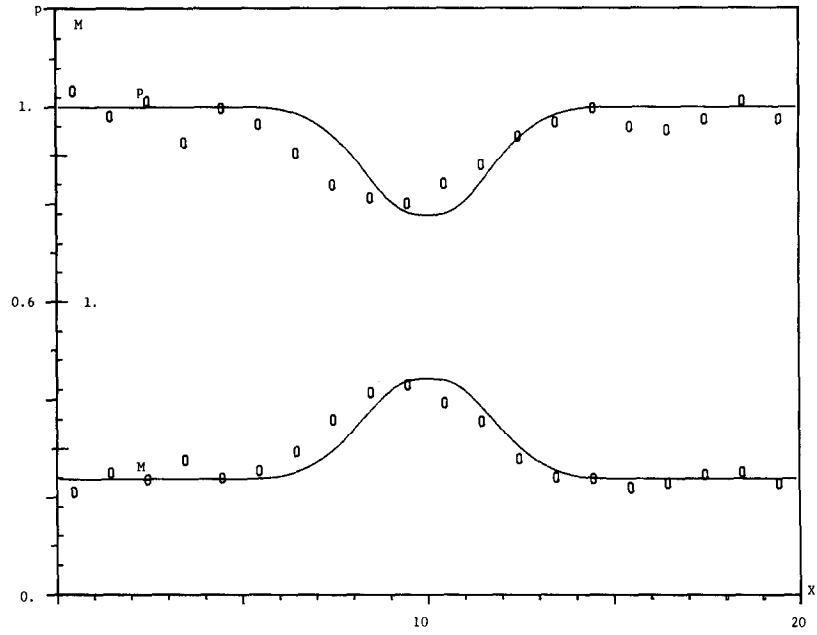

FIG. 6.2. Variation of pressure and Mach number in space at $t = 150$ obtained with Sod's splitting method (coarse mesh).

in the large time limit. The second series involves a transient gas flow which, in the large time limit, approaches a steady-state flow with sonic conditions at the throat section and a normal shock downstream of it. In both series a coarse mesh of 20 grid points and a fine mesh of 60 points were used. The results are compared with the exact solution and with numerical results obtained using Sod's splitting method. The asymptotic steady-state solutions are presented in plots of the variation of the Mach number and pressure in space, superimposed on the exact solution. We describe the transients of the solution by means of contour plots of the pressure in the space–time plane.

The initial conditions for the first series of experiments are presented in Fig. 6.1. They correspond to the exact solution for a piecewise linear nozzle flow with the same inlet, outlet, and throat areas as the sinusoidal nozzle. The boundary conditions in accord with the discussion of Section 5 are: at the inlet section the total temperature and the entropy are fixed, while at the outlet section, the pressure is fixed. Figures 6.2 and 6.3 show the results, at $t = 150$ (375 time steps), obtained with the coarse mesh using Sod's splitting and the generalized random choice methods, respectively. On both graphs the exact solution is superimposed over the numerical solution. We can observe that the random fluctuation of Sod's numerical results is completely

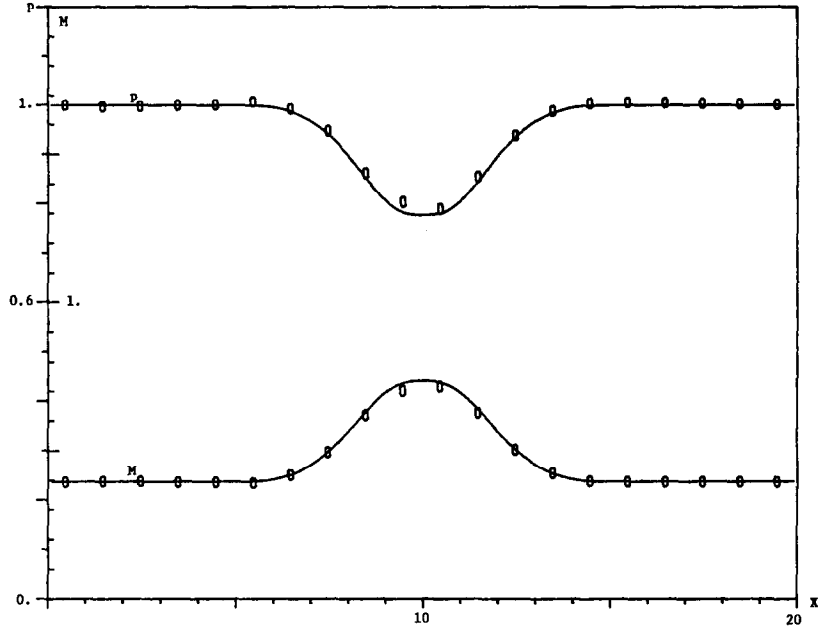

FIG. 6.3. Variation of pressure and Mach number in space at $t = 150$ obtained with the generalized random choice method (coarse mesh).

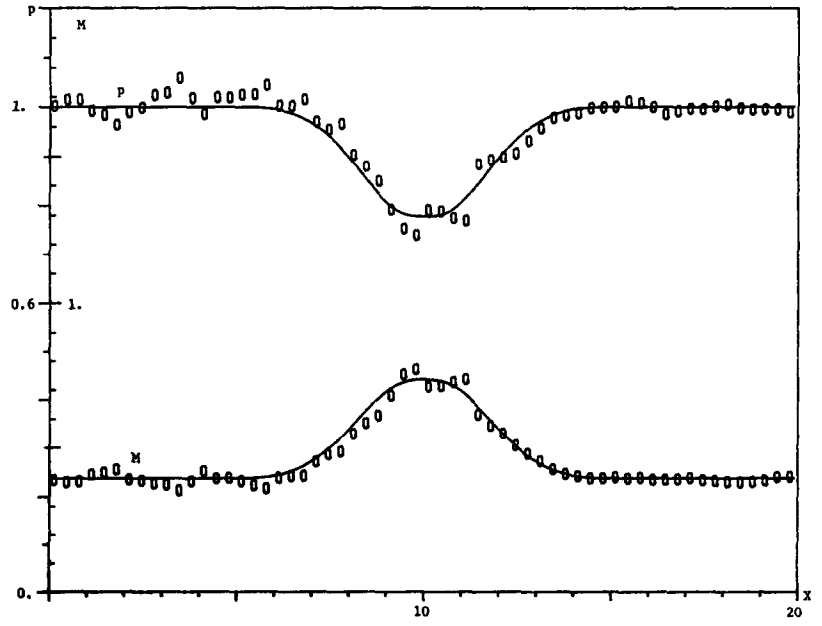

FIG. 6.4. Variation of pressure and Mach number in space at $t = 150$ obtained with Sod's splitting method (fine mesh).

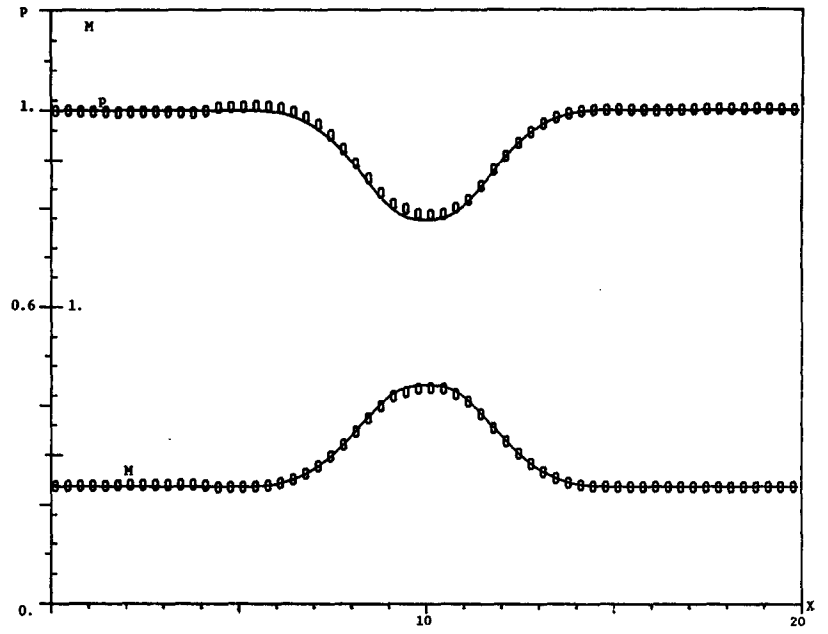

FIG. 6.5. Variation of pressure and Mach number in space at $t = 150$ obtained with the generalized random choice method (fine mesh).

suppressed in the generalized random choice results. The slight discrepancy observed in the zone upstream of the throat in Fig. 6.3 is caused by the fact that steady-state conditions have not yet been reached in that zone. (Note that the signals that travel upstream move more slowly than signals traveling downstream, so that the upstream zone takes more time to reach a steady state.) In Figs. 6.4 and 6.5 we present the solution of the same problem using the fine mesh (1125 time steps). Sod's splitting method gives better results than in the previous run, but the generalized random choice method (even for the coarse mesh) is much superior.

The initial conditions for the second series of runs were intended to simulate the starting conditions of a supersonic blow-down tank. A high-pressure region occupied the whole nozzle except part of the outlet section, where there was a low-pressure region. The boundary conditions are the same as before. The solution of this initial-boundary-value problem consists of transient gas flow which in the large time limit tends to a steady flow with subsonic flow in the inlet, sonic conditions at the throat, and a normal shock downstream of the throat. (With the exit pressure held fixed at 0.7 the shock stands at $x = 13.007$.) We remark that because of the branching of steady-state solutions at the sonic point, as discussed in Section 5, the initial

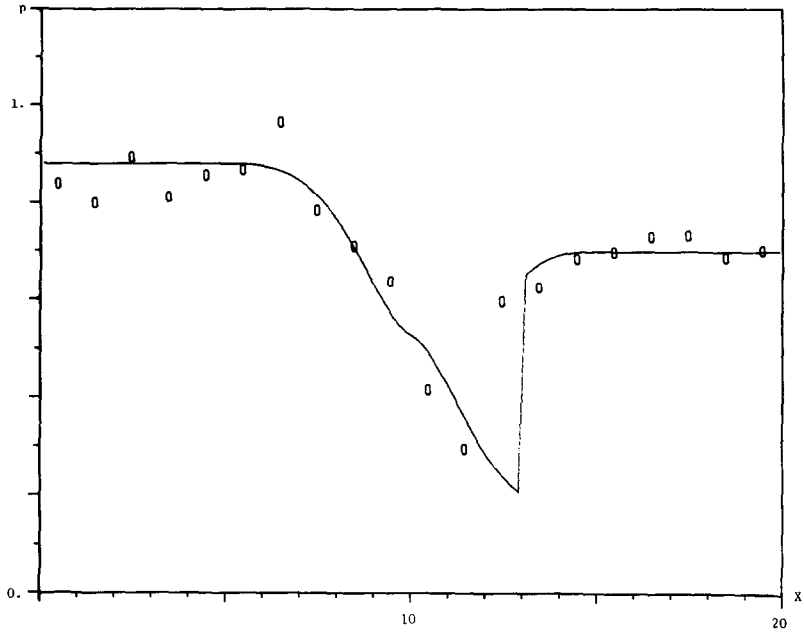

FIG. 6.6a. Variation of the pressure in space at $t = 150$ obtained with Sod's splitting method (coarse mesh).

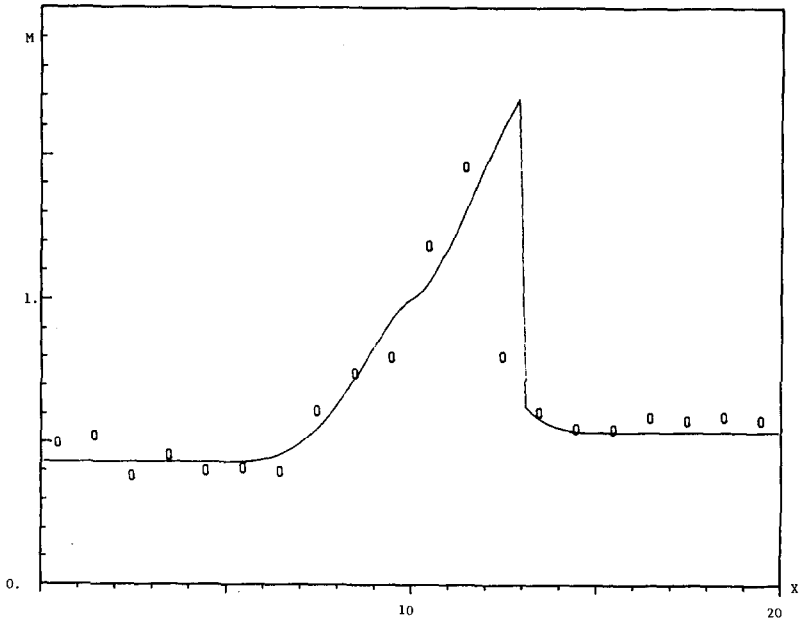

FIG. 6.6b. Variation of the Mach number in space at $t = 150$ obtained with Sod's splitting method (coarse mesh).

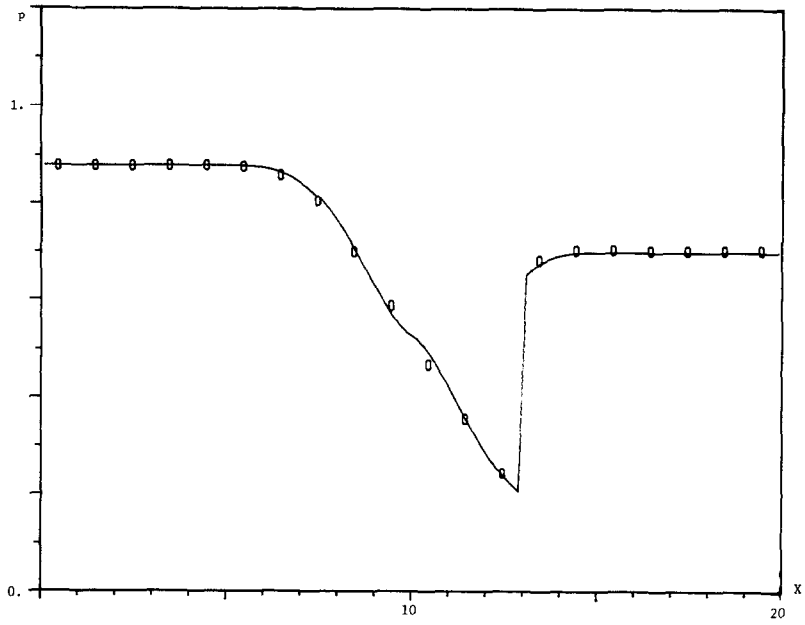

FIG. 6.7a. Variation of the pressure in space at $t = 150$ obtained with the generalized random choice method (coarse mesh).

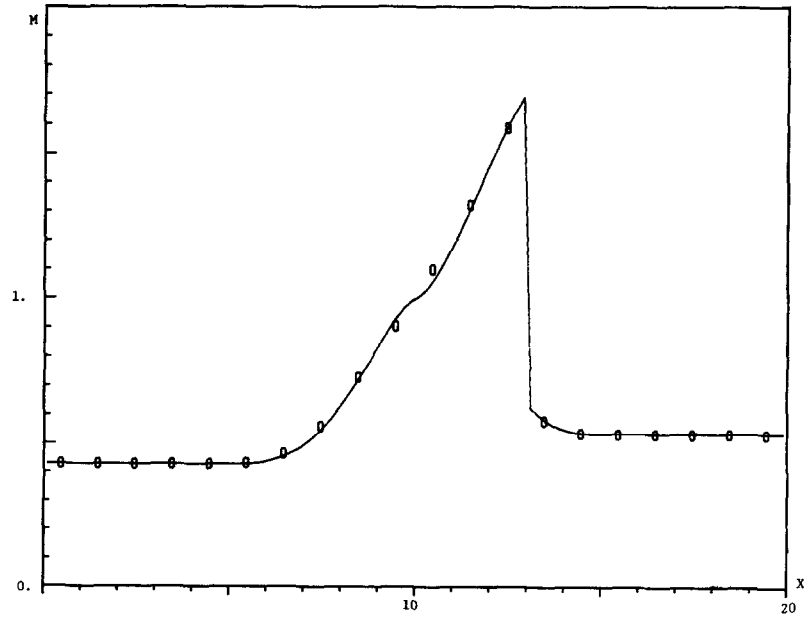

FIG. 6.7b. Variation of the Mach number in space at $t = 150$ obtained with the generalized random choice method (coarse mesh).

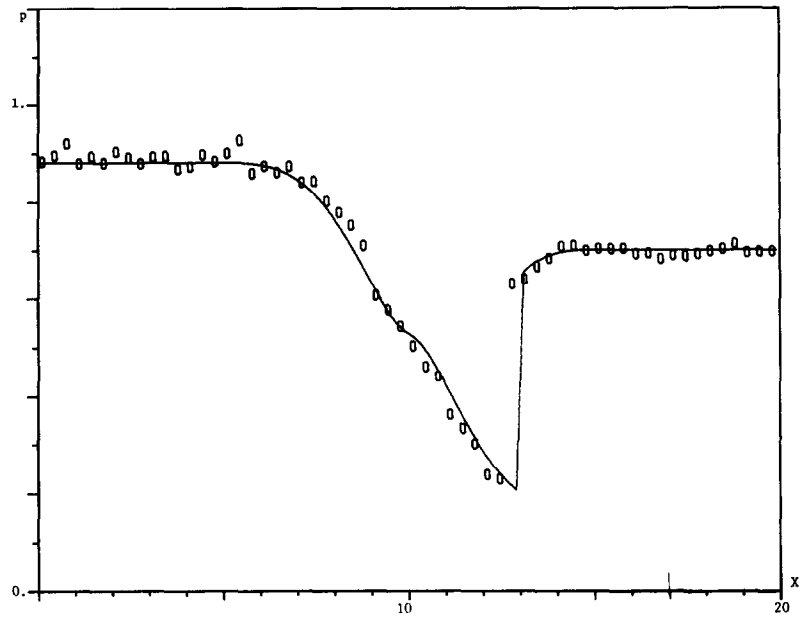

FIG. 6.8a. Variation of the pressure in space at $t = 150$ obtained with Sod's splitting method (fine mesh).

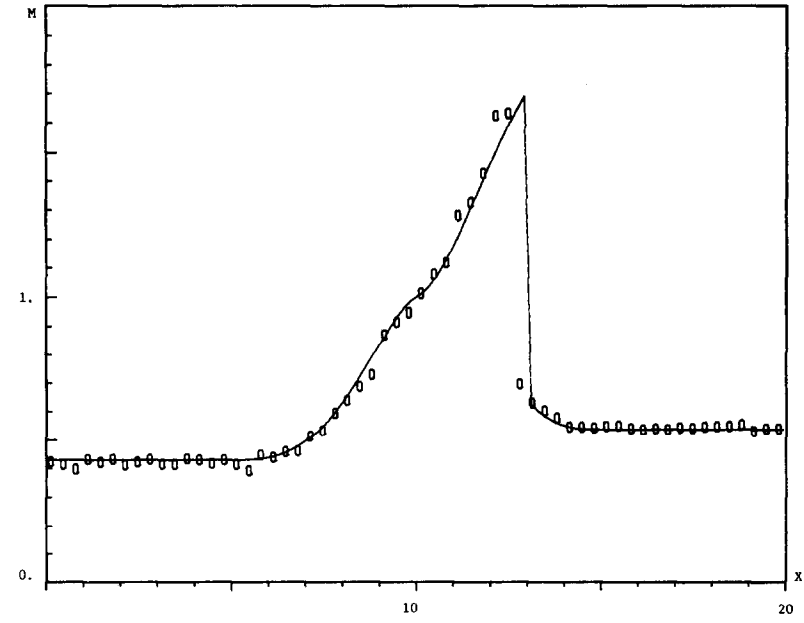

FIG. 6.8b. Variation of the Mach number in space at $t = 150$ obtained with Sod's splitting method (fine mesh).

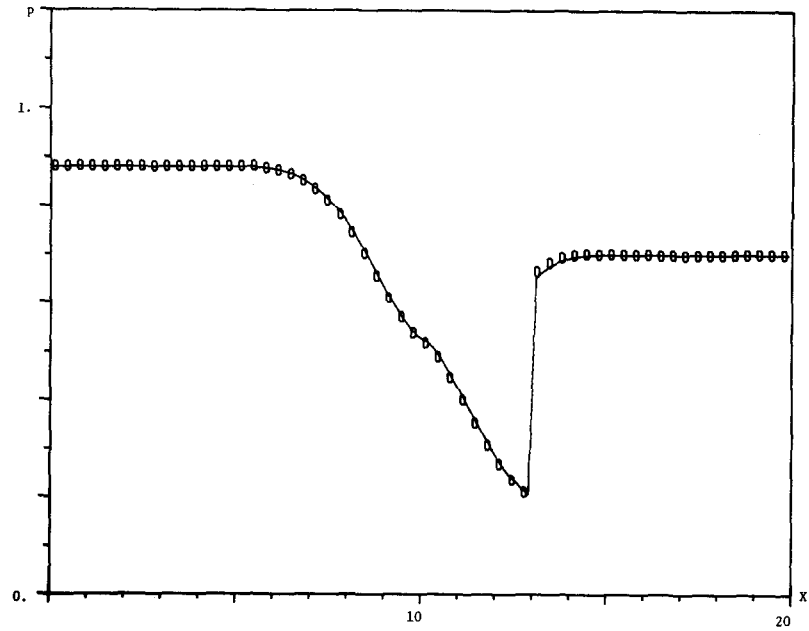

FIG. 6.9a. Variation of the pressure in space at $t = 150$ obtained with the generalized random choice method (fine mesh).

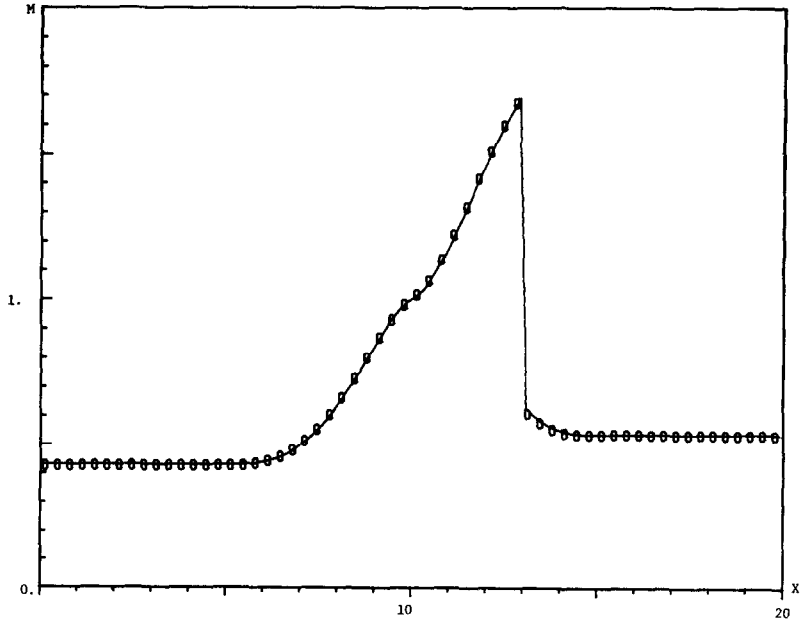

FIG. 6.9b. Variation of the Mach number in space at $t = 150$ obtained with the generalized random choice method (fine mesh).

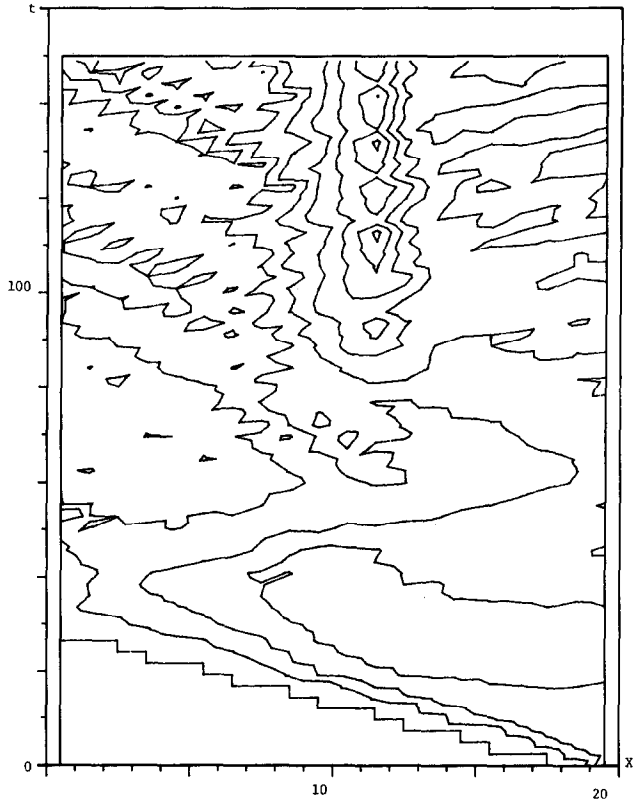

FIG. 6.10. Contour plot of the pressure in space and time obtained with Sod's splitting method (coarse mesh).

conditions chosen are particularly severe for the convergence of the method: the mesh blocks neighboring the throat must use information from the previous time step to determine which branch is to be taken when fitting with steady-state solutions. Figures 6.6a, b and 6.7a, b present the solution, at $t = 150$ (500 time steps), obtained with the coarse mesh using the splitting and the generalized random choice methods, respectively. As expected, Sod's method perfectly resolves the shock. However, downstream of the shock and in the rarefaction wave the random fluctuation diminish the quality of the solution. In contrast, the numerical solution obtained using the generalized random choice method and the exact solutions coincide. The same considerations apply to Figs. 6.8a, b and 6.9a, b obtained with the fine grid (1500 time steps).

In Figs. 6.10 and 6.11 we present contour plots of the pressure in the space–time plane up to time 150.0 for the solution obtained using Sod's

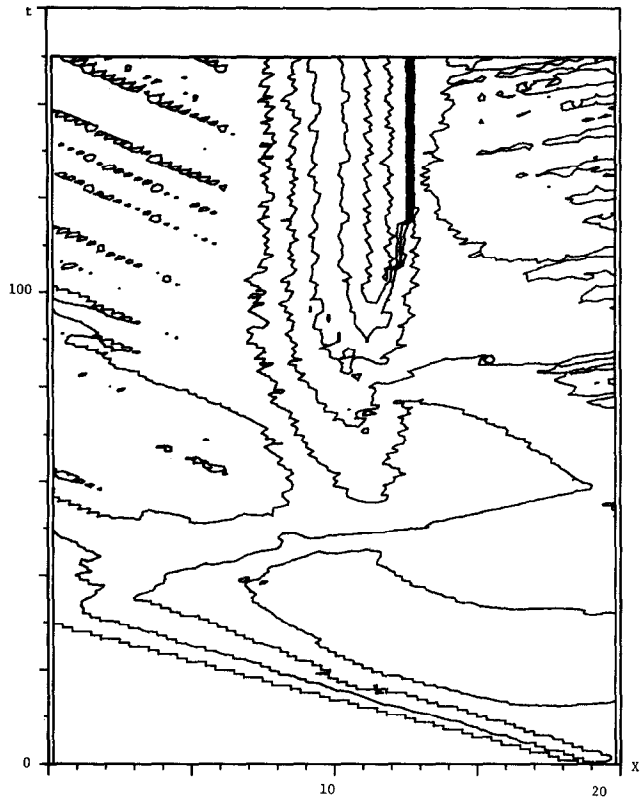

FIG. 6.11. Contour plot of the pressure in space and time obtained with Sod's splitting method (fine mesh).

splitting method with the coarse and fine meshes, respectively. The corresponding results for the generalized random choice method are shown in Figs. 6.12 and 6.13. In both methods the general pattern of the transients of the flow is correctly described: there is a rarefaction wave which travels upstream, partially reflects from the inlet, and finally causes the formation of a stationary shock (which is represented by the closely spaced contour lines). In Sod's method, however, the random fluctuations introduce spurious transients which do not disappear even after a long time. These fluctuations diminish the quality of the asymptotic steady-state solutions. In contrast, the generalized random choice method converges to the asymptotic steady-state solution, and the details of the transients appear to be correct. The fluctuations caused by sampling errors are suppressed in this method because of the better approximation of the solution over mesh intervals.

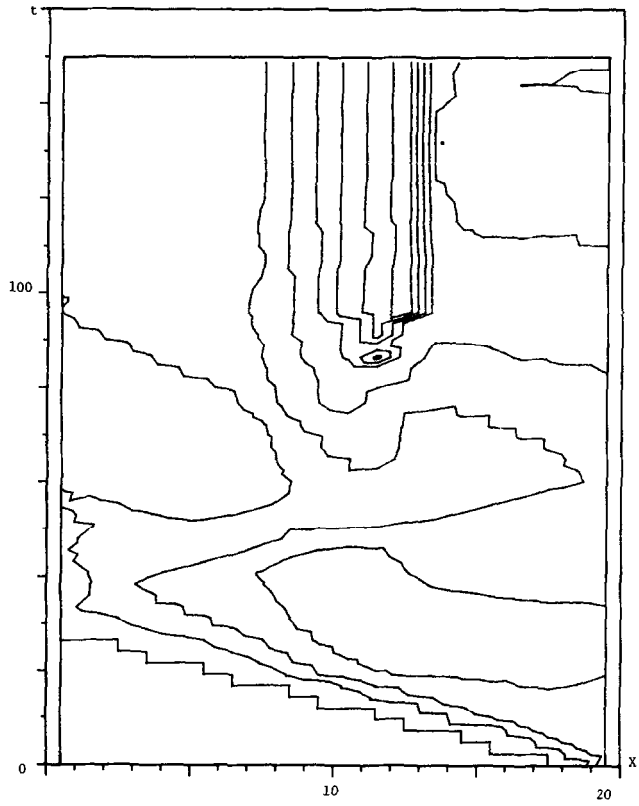

FIG. 6.12. Contour plot of the pressure in space and time obtained with the generalized random choice method (coarse mesh).

Finite difference methods have been widely used to solve nozzle gas flows. Steady-state flows in Laval nozzle were solved using time-asymptotic finite difference methods by Torres and Baker [18], Huang [10], Harten [9], and Bayliss and Turkel [1]. Steady-state flows in divergent nozzles were solved by Harten [9], Colella [4], and Moretti [15] using time-asymptotic methods, and by Shubin *et al.* [16] using a form of Newton's iteration. A comparison with respect to efficiency (computational effort) between the previous results and finite difference calculations is difficult to establish, but qualitative comparison of the results of these authors with our results shows the generalized random choice method to be more accurate than these finite difference schemes for the flows considered.

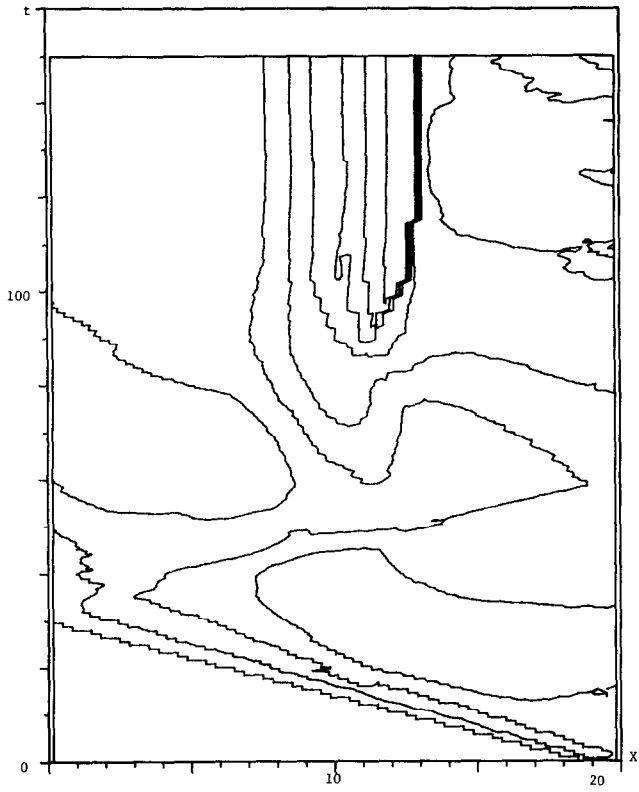

FIG. 6.13. Contour plot of the pressure in space and time obtained with the generalized random choice method (fine mesh).

7. CONCLUSIONS

We have introduced a generalization of the Riemann problem for gas dynamical flows in a variable-area duct, and have used it as a basis for constructing a generalized random choice method. The method was applied to unsteady transonic gas flows in a Laval nozzle where it is shown that the transients and the steady state are correctly described. For nearly steady flows we find this method to be substantially better than other forms of the random choice method and finite difference methods. The generalized random choice method maintains the advantages of the ordinary random choice method, *viz.* high resolution of discontinuities and sharp interfaces and absence of over- and under-shooting phenomena, while remarkably reducing the fluctuation caused by random sampling. This is because for nearly steady flows the solution is better approximated by piecewise steady flows than by piecewise constant flows.

REFERENCES

1. A. BAYLISS AND E. TURKEL, "Far Field Boundary Conditions for Compressible Flows," ICASE Report No. 81-27, NASA Langley Research Center, Hampton, Va., 1981.
2. A. J. CHORIN, *J. Comput. Phys.* **23** (1976), 517.
3. A. J. CHORIN, *J. Comput. Phys.* **25** (1977), 253.
4. P. COLELLA, "A Direct Eulerian MUSCL Scheme for Gas Dynamics," LBL Report No. 14104, University of California, Berkeley (1982).
5. S. K. FOK, "Extension of Glimm's Method to the Problem of Gas Flow in a Duct of Variable Cross-section," Thesis, Department of Mathematics, University of California, Berkeley, 1981.
6. M. P. FRIEDMAN, *J. Fluid Mech.* **8** (1960), 193.
7. M. P. FRIEDMAN, *J. Fluid Mech.* **11** (1961), 1.
8. J. GLIMM, *Comm. Pure Appl. Math.* **18** (1965), 697.
9. A. HARTEN, "High Resolution Schemes for Hyperbolic Conservation Laws," Preprint, 1982.
10. L. C. HUANG, *J. Comput. Phys.* **42** (1981), 195.
11. T. P. LIU, *Comm. Math. Phys.* **68**, (1979), 141.
12. T. P. LIU, "Transonic Gas Flow in a Duct of Varying Area," *Arch. Rat. Mech. Anal.*, in press.
13. G. MARSHALL AND A. N. MENENDEZ, *J. Comput. Phys.* **44** (1981), 167.
14. G. MORETTI, "Thoughts and Afterthoughts about Shock Computations," PIBAL Report 72-37, Polytechnic Institute of Brooklyn, 1972.
15. G. MORETTI, "Numerical Analysis in Gas Dynamics, *in* "Transonic, Shock, and Multi-Dimensional Flows" (R. E. Meyer, ed.), Academic Press, New York, 1982.
16. G. R. SHUBIN, A. B. STEPHENS, AND H. M. GLAZ, *J. Comput. Phys.* **39** (1981), 364.
17. G. A. SOD, *J. Fluid Mech.* **83** (1977), 785.
18. J. A. D. TORRES AND R. C. BAKER, *Comput. Fluids* **7** (1979), 177.